Electronic Supplementary Information for

Mineral Identity, Natural Organic Matter, and Repeated Contaminant Exposures do not Affect the Carbon and Nitrogen Isotope Fractionation of 2,4-Dinitroanisole during Abiotic Reduction

Matthew J. Berens[†], Bridget A. Ulrich[‡], Jennifer H. Strehlau[†], Thomas B. Hofstetter[‡], and William A. Arnold[,†]*

[†]Department of Civil, Environmental, and Geo- Engineering, University of Minnesota, 500 Pillsbury Drive SE, Minneapolis, Minnesota 55455-0116, United States

[‡]Eawag, Swiss Federal Institute of Aquatic Science and Technology, Department of Environmental Chemistry, Überlandstrasse 133, CH-8600 Dübendorf

[*]Corresponding author: William A. Arnold; Phone: 612-625-8582; e-mail: arnol032@umn.edu

12 Pages, 5 Figures

Contents

S1 Chemical Sources and Analytical Methods

S1.1 Materials

All aqueous solutions were prepared in ultrapure Milli-Q water (18.2 MΩ•cm) that was first deoxygenated by bubbling with N_2 gas (99.99%, Matheson) for at least 2 h. $Na_2S•9H_2O$ (≥98%), $Fe(NO_3)_3•9H_2O$ (≥98%), methanol (ACS grade), $NaHCO_3$ (ACS grade), $FeSO_4•7H_2O$ (ACS grade), KNO_3 (≥99%), and HCl (trace metals grade) were purchased from Sigma. $FeCl_2•6H_2O$ (ACS grade), HCl (ACS grade), NaOH (ACS grade), KOH (ACS grade), H_2SO_4 (ACS grade), acetonitrile (HPLC grade), ferrozine (B-(2-pyridyl)-5,6-bis(4-sulfophenyl)-1,2,4-triazine disodium salt hydrate, >98%), and NaCl (ACS grade) were purchased from Fisher. All glassware, cuvettes, stir bars, and Nalgene bottles were soaked in 0.1 M oxalic acid (pH 3.5) for at least 2 days and rinsed with ultrapure water prior to use to remove any residual iron. Elliot Soil Humic Acid (ESHA, Cat. No. 4S102H) was purchased from the International Humic Substances Society (IHSS) in St. Paul, MN. Elemental composition was performed by the IHSS and characterized the ESHA sample as 7.62% (w/w) water, 0.44% (w/w) ash, and 59.51% (w/w) C. Solutions containing ESHA were prepared to 5 mg/L as organic carbon.

S1.2 Ferrozine Assay for Determining Fe(II) Content

The Fe(II) content was determined by the method of Viollier et al.[1] Aliquots from the batch reactors were filtered with a 0.2 μm PTFE syringe filter. To measure the Fe(II) content, 0.10 mL of reaction filtrate was transferred to a clean, dry polystyrene cuvette with 2.70 mL deoxygenated, ultrapure water and 0.20 mL of a 5 g/L aqueous ferrozine solution. Each sample was capped, mixed by inversion, and the absorbance was measured at 562 nm using a Shimadzu UV-1601PC UV-Vis spectrophotometer. A five-point calibration curve was constructed by producing serial dilutions from 0.0–0.005 mM Fe(II) in ultrapure water. A ferrozine/ultrapure water solution was used as the blank. The Fe(III) content of a sample can also be quantified by the ferrozine assay by using hydroxylamine hydrochloride to reduce the Fe(III) to Fe(II). The difference between the measurements with and without hydroxylamine give the Fe(III) value.

S1.3 HPLC Method

Aqueous DNAN, MENA, and DAAN concentrations were quantified by an Agilent Technologies 1200 Series HPLC equipped with an photodiode array and an Inertsil ODS-3 column (4.6 × 250 mm, 5 μm particle size). The mobile phase (60 % acetonitrile/40 % ultrapure water) was operated at a flow rate of 1.00 mL/min. The injection volume was 20 µL. A five-point calibration curve was produced for DNAN from 0.01–0.2 mM. The typical retention times with this method were approximately 4.2 min, 5.8 min, and 7.0 min for DAAN, MENA, and DNAN, respectively. The detection wavelength was 230 nm.

S2 Mineral Synthesis and Analysis

S2.1 Mineral Synthesis Procedures

The mackinawite synthesis method was adapted from Butler and Hayes.[2] One-hundred and twenty (120) mL of 1.1 M $Na_2S•9H_2O$ were added to 200 mL of 0.57 M $FeCl_2•6H_2O$ and stirred for 3 days. The particle suspension was then equally divided into two dialysis bags (Spectrum Laboratories Inc., molecular weight cut off = 2000 g/mol) and placed in fresh, deoxygenated, ultrapure water three times per day for three days. Following dialysis, the mineral suspensions were combined and stored in a 500 mL Nalgene bottle. The particle density in suspension was determined as 33.3 g/L.

The goethite synthesis method was adapted from Anschutz and Penn.[3] First, a ferrihydrite suspension was produced by adding 1 L of 0.48 M $NaHCO_3$ dropwise to 1.0 L of 0.40 M $Fe(NO_3)_3•9H_2O$ with constant stirring. The resulting suspension was transferred to 250 mL Nalgene bottles and microwaved in 30 s intervals until boiling occurred with venting and shaking between each interval. Once boiling was achieved, the suspensions were submersed in an ice bath until the suspension temperature reached 20 °C and then transferred into dialysis bags and placed in fresh, deoxygenated, ultrapure water three times per day for three days. Following dialysis, the pH of the suspension was adjusted to 12 with 5 M NaOH and aged at 90 °C for 72 h. Approximately 400 mL of the supernatant were discarded to concentrate the goethite particles after aging. The counter-ions in the goethite suspension were removed by dialysis according to the previously described method.[3] The particle density in suspension was determined as 10 g/L.

The magnetite synthesis method was adapted from Schwertmann and Cornell.[4] An $FeSO_4$ solution was prepared by dissolving 40 g of $FeSO_4 \bullet 7H_2O$ in 280 mL of ultrapure water in a 0.5 L separation flask. A KNO_3/KOH solution was prepared by first dissolving 3.23 g of KNO_3 in 120 mL of ultrapure water in a 250 mL beaker. Slowly, 22.4 g of KOH were then added to the KNO_3 solution. The separation flask was placed in a 90 °C water bath and allowed to equilibrate with constant stirring. Both the separation flask and 250 mL beaker were covered with aluminum foil and bubbled under N_2. The KNO_3/KOH solution was then transferred to a buret and added to the $FeSO_4$ solution by piercing the foil above the $FeSO_4$ with the buret tip and adding dropwise. Once all the solution had been added and a black precipitate had formed, the solution was allowed to continue stirring for 45 min under constant N_2 bubbling. The solution was then cooled and transferred to an anaerobic glovebag. The particles were washed three times by centrifugation, dried, and stored in the glovebag.

S2.2 Mineral Characterization Methods

X-Ray diffraction (XRD) patterns were collected using a PANanalytical X'Pert Pro X-ray diffractometer equipped with a cobalt source (1.79 Å) and an X'Celerator detector. Patterns were collected from 20° to 80° 2θ over 60 min and compared to powder diffraction files (PDF) No. 29-0713 (goethite), No. 19-0629 (magnetite), and No. 15-0037 (mackinawite). Prior to analysis, each mineral suspension was washed three times via centrifugation with ultrapure water to remove any salts, dried, and finely ground using a mortar and pestle. XRD patterns of the as-synthesized minerals are provided in Figure S1.

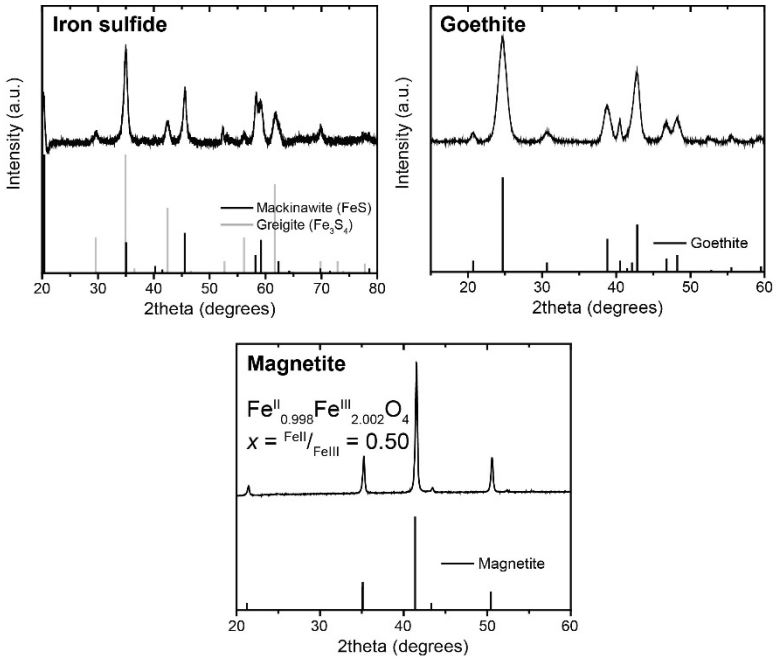

Figure S1. XRD patterns for synthetic iron sulfide (mackinawite), goethite, and magnetite.

Surface areas were determined by nitrogen adsorption analyses and calculated using the Brunauer-Emmett-Teller (BET) adsorption model.[5] Measurements were performed between 0 and 0.3 P/P_0 using a Quantachrome Autosorb iQ analyzer. Samples were outgassed at 100 °C for 12 h prior to analysis.

Mass loading experiments were performed to determine mass of particles per suspension volume for goethite and mackinawite. Five total aliquots (0.1–0.5 mL) of each suspension were added to separate weigh boats of known mass and dried at room temperature until no liquid remained. Particle densities were then calculated by fitting the mass of dried solid against aliquot volume with a linear regression model.

S3 Control Experiments for DNAN Transformation Kinetics

A control experiment was performed to determine if DNAN transformation occurs in the absence of a mineral phase. Reactors were prepared in triplicate with bicarbonate buffer (10 mM,

pH 7), Fe(II) (1 mM), and DNAN (0.2 mM). The results (Figure S2) revealed that no DNAN transformation occurred without an associated mineral phase after 21 days.

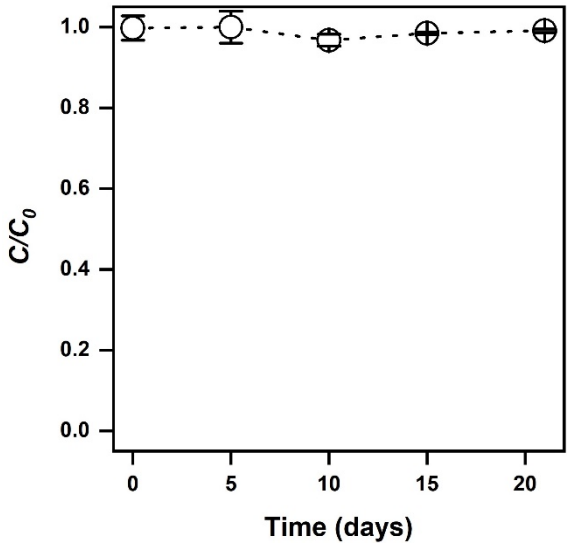

Figure S2. Control experiment for DNAN transformation without an added mineral. No DNAN transformation was observed in the control reactor with aqueous Fe(II) as compared to systems containing an Fe-bearing mineral (see Figure 1). Reactors were prepared according to the methods described in the main text. Error bars represent standard deviations in triplicate reactors.

S4 CSIA Data Analysis

S4.1 Calculation of Isotope Fractionation Parameters

Carbon and nitrogen isotope signatures, $\delta^{13}C$ and $\delta^{15}N$, were calculated according to eq. S1 from $^{13}C/^{12}C$ and $^{15}N/^{14}N$ measurements performed using SPME coupled to GC/IRMS.[6,7]

$$\delta^{h}E = \frac{R(^{h}E/^{l}E)_{sample}}{R(^{h}E/^{l}E)_{reference}} - 1 \qquad (S1)$$

$R(^{h}E/^{l}E)_{sample}$ and $R(^{h}E/^{l}E)_{reference}$ are the ratios of the heavy (h) and light (l) isotopes of the element, E. Isotope enrichment factors for DNAN were then derived from log-linear regression of eq. 1 (see main text). Carbon and nitrogen apparent kinetic isotope effects, ^{13}C-AKIE and ^{15}N-AKIE, were then calculated according to eq. 2 (see main text)[8] where $z = 1$ for ^{13}C-AKIE and $z = 2$ for ^{15}N-AKIE. It should be noted that values of ε_E obtained from eq. 1 are bulk enrichment values

whereas values used to calculate ^{n}E-AKIEs from eq. 2 are specific for the reactive position (i.e., $\varepsilon_{\text{reactive position}}$). The differences in these values account for intermolecular and intramolecular competition which can lead to "isotopic dilution" and subsequent decreases in observed fractionation values. For simplicity, we did not make this distinction in the main text but ε_{E} values provided in the main text are for $\varepsilon_{\text{reactive position}}$. See refs 9 and 10 for a detailed description of how this correction is made.[9,10]

S4.2 Detailed Carbon Fractionation Results

In the main text (Figure 3) all isotope fractionation results are plotted together, for simplicity, because minimal fractionation was observed across all sample sets. Here, values of $\delta^{15}N$ and $\delta^{13}C$ vs. C/C_0 (Figure S3) are provided separately for each combination of reaction condition and mineral type.

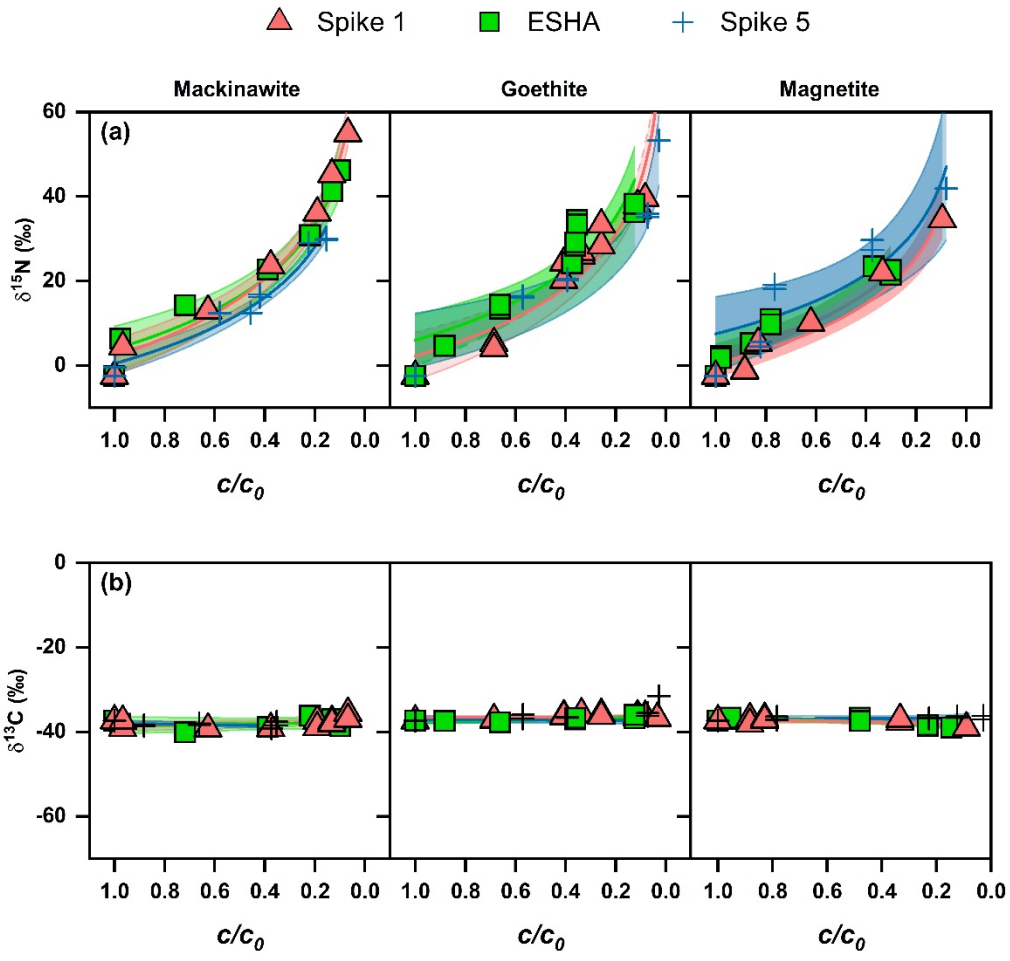

Figure S3. Complete (a) N and (b) C isotope fractionation results for abiotic reduction of DNAN calculated using nonlinear regression analyses of eq.1. All shaded regions represent 95% confidence intervals for each data set.

S4.3 Decreased Enrichment Factors during Repeated Contaminant Exposure

A general trend of slightly reduced N fractionation was observed over 5 sequential DNAN spikes (Figure S4). Several factors may contribute to this result and we hypothesize the observed effects to be caused by the evolution of mineral surfaces. For example, Chun et al.[11] observed the oxidative growth of goethite nanoparticles during the reduction of 4-chloronitrobenzene in sequential-spike batch reactions containing Fe(II)/goethite, similar to those in the present study. Even though particle growth had occurred, the newly formed surfaces displayed marked increases in roughness leading to decreased mineral reactivity and negligible (even decreases on some facets) changes in surface area. Losses in reactivity were attributed to a lower Fe(II) uptake capacity of the roughened surfaces (approximately 16% decrease over five spikes). In addition, changes in mineral morphology may inhibit proton and electron transfer reactions that occur prior to the initial N—O bond cleavage. These transfer reactions typically elicit isotope effects that are minute in comparison to N—O bond cleavage but may be diminished over multiple contaminant reductions as the mineral evolves resulting in decreased total isotope enrichment.[12] The trends in reductive pathways ($\varepsilon_N \approx$ -19 to -9 ‰ and $\varepsilon_C \approx$ -0.1 to -1.5 ‰), however, are still easily distinguished from oxidation ($\varepsilon_N = -2.7 \pm 0.4$ ‰ , $\varepsilon_C = -6.0 \pm 0.5$ ‰ and ε_N = -3.2 to -2.5 ‰ , ε_C = -3.7 to 2.8 ‰ for alkaline hydrolysis and biodegradation, respectively).[13]

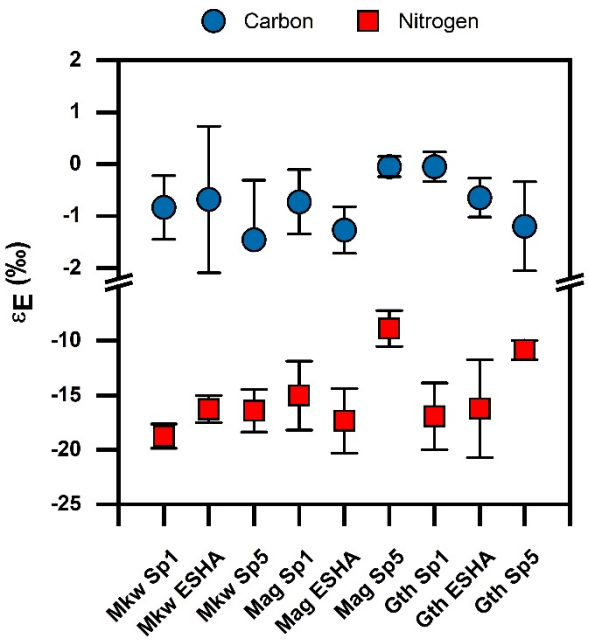

Figure S4. Carbon and nitrogen isotope enrichment factors (ε_E) in mackinawite (Mkw), magnetite (Mag), and goethite (Gth) suspensions derived using log-linear regression of eq. 1. Error bars represent the 95% confidence intervals.

S4.4 Two-Dimensional Isotope Analysis

In the main text (Figure 5), the results of two-dimensional CSIA are provided with all reduction data combined. These same data are presented in Figure S5 with the reduction data separated by mineral type to indicate that isotope fractionation in each mineral suspension followed the same trend.

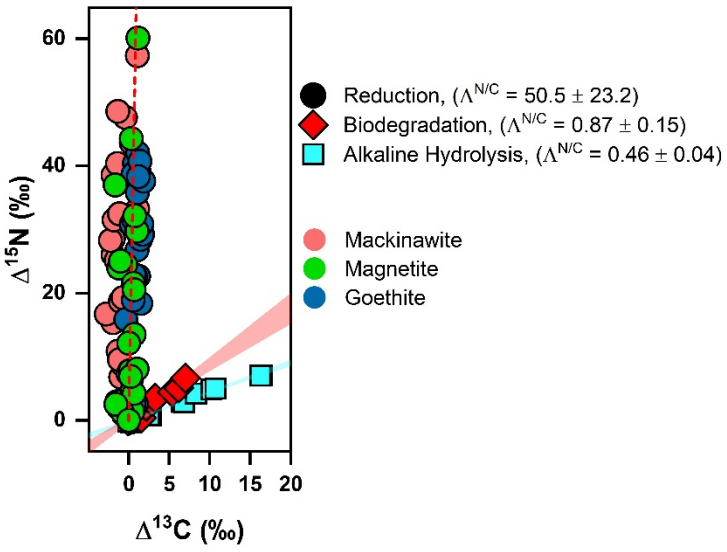

Figure S5. Two-dimensional isotope fractionation for reductive and oxidative DNAN transformation pathways. Isotope fractionation observed during abiotic reduction (circles) is shown with respect to the mineral type and compared to alkaline hydrolysis (squares), and biodegradation (diamonds). Alkaline hydrolysis and biodegradation data were reproduced with permission from Ulrich et al.[13]

S5 References

1 E. Viollier, P. W. Inglett, K. Hunter, A. N. Roychoudhury and P. Van Cappellen, The ferrozine method revisited: Fe(II)/Fe(III) determination in natural waters, *Appl. Geochemistry*, 2000, **15**, 785–790.

2 E. C. Butler and K. F. Hayes, Effects of solution composition and pH on the reductive dechlorination of hexachloroethane by iron sulfide, *Environ. Sci. Technol.*, 1998, **32**, 1276–1284.

3 A. J. Anschutz and R. L. Penn, Reduction of crystalline iron(III) oxyhydroxides using hydroquinone: Influence of phase and particle size, *Geochem. Trans.*, 2005, **6**, 60–66.

4 U. Schwertmann and R. M. Cornell, in *Iron Oxides in the Laboratory: Preparation and Characterization*, Wiley-VCH Verlag GmbH, Weinheim, Germany, 2nd edn., 2000, pp. 135–140.

5 S. Brunauer, P. H. Emmett and E. Teller, Gases in multimolecular layers, *J. Am. Chem. Soc.*, 1938, **60**, 309–319.

6 M. Berg, J. Bolotin and T. B. Hofstetter, Compound-specific nitrogen and carbon isotope analysis of nitroaromatic compounds in aqueous samples using solid-phase microextraction coupled to GC/IRMS, *Anal. Chem.*, 2007, **79**, 2386–2393.

7 S. Spahr, S. Huntscha, J. Bolotin, M. P. Maier, M. Elsner, J. Hollender and T. B.

Hofstetter, Compound-specific isotope analysis of benzotriazole and its derivatives, *Anal. Bioanal. Chem.*, 2013, **405**, 2843–2856.

8 T. B. Hofstetter, P. Schwarzenbach and S. M. Bernasconi, Assessing transformation processes of organic compounds using stable isotope fractionation, *Environ. Sci. Technol.*, 2008, **42**, 7737–7743.

9 L. Melander and W. H. Saunders, *Reaction Rates of Isotopic Molecules*, John Wiley & Sons, New York, 1980.

10 M. Elsner, L. Zwank, D. Hunkeler and R. P. Schwarzenbach, A new concept linking observable stable isotope fractionation to transformation pathways of organic pollutants, *Environ. Sci. Technol.*, 2005, **39**, 6896–6916.

11 C. L. Chun, R. L. Penn and W. A. Arnold, Kinetic and microscopic studies of reductive transformations of organic contaminants on goethite, *Environ. Sci. Technol.*, 2006, **40**, 3299–3304.

12 A. E. Hartenbach, T. B. Hofstetter, M. Aeschbacher, M. Sander, D. Kim, T. J. Strathmann, W. A. Arnold, C. J. Cramer and R. P. Schwarzenbach, Variability of nitrogen isotope fractionation during the reduction of nitroaromatic compounds with dissolved reductants, *Environ. Sci. Technol.*, 2008, **42**, 8352–8359.

13 B. A. Ulrich, M. Palatucci, J. Bolotin, J. C. Spain and T. B. Hofstetter, Different mechanisms of alkaline and enzymatic hydrolysis of the insensitive munition component 2,4-dinitroanisole lead to identical products, *Environ. Sci. Technol. Lett.*, 2018, **5**, 456–461.